Journal of Thermal Analysis and Calorimetry (2019) 137:1877–1890
https://doi.org/10.1007/s10973-019-08095-x

Using isothermal calorimetry, X-ray diffraction, thermogravimetry and FTIR to monitor the hydration reaction of Portland cements associated with red mud as a supplementary material

Roberto Cesar de Oliveira Romano[1] · Heitor Montefusco Bernardo[1] · Marcel Hark Maciel[1] · Rafael Giuliano Pileggi[1] · Maria Alba Cincotto[1]

Received: 12 June 2018 / Accepted: 14 February 2019 / Published online: 2 March 2019
© Akadémiai Kiadó, Budapest, Hungary 2019

Abstract
This study is part of a global project to find some large-scale application for red mud. A previous work confirmed that the use of RM as partial substitution for cement can affect its rheological properties; however, it is possible to produce cementitious materials without lose mechanical performances at harden state. The main goal of the work was to assess the impact of red mud (RM) as replacement of different Brazilian Portland cements by monitoring the formation of hydrated products over time, by thermogravimetry, X-ray diffraction and FTIR. Results show that the presence of RM increases the induction period, the gypsum and portlandite consumption as well as the amount of ettringite and monosulfoaluminate produced. The formation of sodium silicoaluminate hydrate (NASH) was also observed, regardless the kind of cement, as a result of the reaction with aluminates and silicates from the binder.

Keywords Red mud · Portland cement · Hydration reaction

Introduction

Nowadays, Portland concrete is worldwide the most produced and consumed construction material in modern society. Its yearly production is estimated to be higher than 10 km^3. Basically, these cementitious products consist of a mixture of aggregates, binder and water. Although it is not possible to obtain an exact value for the volume produced, the value above is estimated in terms of the production of Portland cement. In this case, this hydraulic binder reached the expressive mark of 4 billion tons/year between 2013 and 2014 [1–3].

Currently, the cement industry is under pressure to mitigate the CO_2 emission worldwide, because their current global release accounts for approximately 7% in global warming [4, 5]. Moreover, the main challenge for the future will be to increase the production of the most important building materials without intensifying the impact of the enormous volumes produced.

Considering only the aspects related to materials, different routes have been developed to replace clinker with the use of alternative materials such as:

1. A by-product of a few industrial processes (as ground blast furnace slag, fly ash, silica fume, etc.);
2. Inert materials (as limestone filler);
3. A new kind of cement with a lower environmental impact.

For this reason, the level of efficiency currently practiced in cement technology has been investigated to identify new opportunities to increase its production without increasing cement production.

By the same token, the search for a large-scale application for red mud, a waste material resulting from the Bayer process to obtain alumina from bauxite ore, poses itself as a great challenge. For a long time, the material has been disposed of into mud lakes, bringing about considerable environmental impact [5–15].

In this process, the bauxite ore is crushed, milled and heated at up to 200 °C in a pressure vessel together with a

✉ Roberto Cesar de Oliveira Romano
rcorjau@gmail.com

[1] Department of Civil Construction Engineering, University of São Paulo, Av. Prof. Almeida Prado, trav. 2, n° 83, São Paulo, SP CEP: 05424-970, Brazil

sodium hydroxide solution. The solution of aluminum-rich components remains in the process, while the residue is separated by filtering and disposed off into mud lakes, creating an environmental hazard because of its alkalinity and its potential ability to leach soluble ions.

Despite some controversies, and even with a precise control of lake contention, there will always be a risk of disruption, as the event that occurred in October 2010, in Hungary, killing ten people and contaminating a large area [5].

For that reason, the efforts to find an application for this waste have been stepped up in recent years, focusing on water treatment, soil recovery, production of structural materials with cement, production of red ceramics, metal coating, production of pozzolanic pigments, treatment of waste from gold mines, selective filtering of SO_2 or H_2S, corrosion inhibitor in Fe–C alloys, support for catalysis, and others [5–16].

However, the current cost of disposal is estimated at $4–12/ton, which is rather low and part of the difficulty in attaining a viable commercial solution for such waste generation challenge. Those materials pose many challenges, and a major problem is that they may show a great deal of variation from site to site, and, in some cases, a solution that may prove to be adequate for one site may be inadequate for the other [2, 7].

A cement industry roadmap has identified that:

1. The partial replacement of cement or its main component (clinker) by alternative raw materials (known as supplementary cementitious materials or SCM) has the most promising potential to help them achieve their global target of reducing CO_2 per ton of cement from 750 to 420 kg by 2050 [3],
2. The growth rate of cement production will not proceed at the same rate as the availability of regular SCM (blast furnace slag, fly ash, natural pozzolans, limestone, and others);

there is an immediate need to develop new SCM or use them more efficiently [1].

In this scenario, the partial substitution of Portland cement for red mud would be an alternative to obtain a large-scale application for the waste. The development of a new supplementary material to the binder enables the reduction in cement consumption and, consequently, a decrease in CO_2 emission [2, 5, 6, 8, 10].

This work is part of a global project which showed that the use of red mud affects the rheological properties of cementitious compositions, but the hardened state properties of mortar, concrete and hydraulic tiles are not deteriorated. This work is the result of monitoring the chemical reaction of different Brazilian Portland cements associated with the same red mud in an effort to understand the interactions between the residue and different binders in the formation of hydrated products.

Experimental

Materials

All pastes were formulated using red mud, collected in the plant of alumina/aluminum production of Alcoa Latina America, in Poços de Caldas, southeast Brazil, and Brazilian Portland cements, named according national standards as CPI, CPV, CPIIF and CPIII.

Mixing procedure and sample preparation

All compositions were mixed maintaining constant the water-to-solid ratio (0.5) and the cement-to-RM ratio in the blended compositions (90:10, in mass). The dry powder was placed into a beaker and then the whole amount of water added. The waiting time to ensure the complete wetting of the powder was 1 min; then, the mixing started maintaining the rotational speed of the stirrer at 10,000 rpm for 2 min.

Part of this paste was used to monitor the heat release using isothermal conduction calorimetry and setting time by Vicat needle penetration test (see "Methods" section), whereas the remaining part was distributed in plastic cups (specimens cured at 23 °C and 70% of relative humidity). The hydration of those specimens was stopped at desired times to quantify the hydrated products by X-ray diffraction, thermogravimetry and FTIR tests:

- After 1, 2, 4, 8, 24 and 48 h, the cement hydration was stopped by immersing each sample in liquid nitrogen for 2 min. After the freezing process, the samples were conditioned in a freezer at temperature below − 25 °C, to prevent further reaction, and then, lyophilized for 24 h in a Terroni Fauvel, equipment model LC1500. In that step, the free water was adsorbed, and part of the frozen interlamellar on the paste structure was eliminated by sublimation. After lyophilization, the samples were placed in a desiccator with silica gel and maintained under vacuum until the execution of each test [17]. After all the tests, the samples were ground in a pestle and sieved in a sieve #200 mesh. The passing material—particles smaller than 75 μm—was used for the analyses.

It is important to highlight that the freeze-drying method is not the best procedure to quantify the hydrated compounds; as reported in the literature, this method does not well preserve the calcium aluminate hydrates (ettringite, AFm) [18]. However, as the results obtained in this work can be discussed comparatively, we kept this monitoring even knowing about this difficultly, but it is recommended

for future works the hydration stoppage using the solvent exchange (isopropanol/ether) method.

Methods

Isothermal conduction calorimetry

The heat release during the cement hydration reaction was quantified using an isothermal calorimeter, TAM Air, TA Instruments, with a precision of ± 20 μW, for 48 h. After mixing, as described above, the paste was put into an ampoule and sealed; the data acquisition was initiated 5 min after the addition of the water to the powder.

Vicat needle penetration test

The tests were carried out at 23 °C, according to the technical standard NBR NM 65/03—Portland cement—Determination of setting time, in a modified Vicat apparatus, ELE. The method consists in the penetration of a needle into the cement paste, with the beginning of the setting annotated when the needle stops at 0.5 mm from the bottom, and the final setting annotated when the needle stops at 38 mm from the bottom (2 mm from the top). The needle penetration control was performed each 15 min. It was decided to perform the tests according to the Brazilian technical standard because the cements used are binders that meet the Brazilian requirements.

X-ray diffraction

Changes in the mineralogical phases formed over time were monitored by means of X-ray diffraction, in a X'Pert Philips equipment, using copper $K\alpha 1$ (θ = 1.54 Å), step of 0.02° every 100 s, at a diffraction angle range of 2.5–70°θ.

Thermogravimetric analysis

A thermobalance Libra 209 F1, Netzsch, was used to monitor the thermal decomposition of hydrated products, in N_2 atmosphere, from 30 to 1000 °C at a heating rate of 10 °C per minute.

Fourier transform infrared spectroscopy

The tests were performed using an equipment Nicolet, Thermo Scientific, model Nexus 6700.

Results

Characterization of raw materials

Table 1 shows the chemical characteristics of different Portland cements and red mud, obtained by wet chemical analysis and atomic absorption, respectively. Those binders are in accordance with Brazilian standards and, as

Table 1 Chemical characterization of Portland cements and red mud

Determinations	CPI	CPV	CPIIF	CPIII	RM
Loss on ignition (LOI)	2.16	3.38	12.5	2.27	14.1
SiO_2	19.7	19.6	14.8	29.8	20.2*
CaO	65.5	64.1	56.2	49.6	3.83*
MgO	0.71	0.79	6.31	4.55	< 0.1*
Fe_2O_3	3.40	3.19	3.25	1.69	22.6**
Al_2O_3	5.30	5.35	4.64	9.72	25.0**
Mn_2O_3	Undetermined				0.42*
TiO_2					3.37*
SO_3	2.23	2.82	3.16	1.32	und
Na_2O	< 0.1	0.14	< 0.1	< 0.1	**8.78**
K_2O	0.64	0.71	0.26	0.50	2.26*
Alkaline equivalent (in Na_2O)***	0.45	0.61	0.19	0.63	10.3*
Free lime (CaO)	1.57	1.75	1.48	0.98	Undetermined
S^{2-}	und	und	< 0.1	0.63	
Insoluble residue (IR)	0.22	0.78	3.17	0.23	
CO_2	0.53	2.05	10.7	1.30	

und, undetermined

*Result obtained by atomic absorption

**Result obtained by complexometry

***Alkaline equivalent (in Na_2O) = Na_2O + 0.658 K_2O

expected, the highest amount of volatile was observed in CPIIF, due to decarbonation, as it contains approximately 10% of limestone filler (calcite and dolomite). CPIII presented a higher amount of silica and aluminum resulting from blending with almost 65% of ground blast furnace slag.

The amount of chemical species as quantified in CPI and CPV is similar, with a higher calcium content than the others. However, the loss on ignition (LOI) was a little higher in CPV due to the addition of limestone filler during the binder production

Red mud contains a high amount of iron, aluminum and silicon oxides and an alkaline equivalent higher than 10% because it has more than 8.7% of Na_2O presence from the ore digestion with caustic soda. This value was highlighted in Table 1 because the alkalis content is one of the most important challenges to find a large-scale application for this residue. A higher loss on ignition is also observed due to the presence of bound water and carbonates.

Figure 1 illustrates a ternary diagram of $CaO–SiO_2–Al_2O_3$, indicating the proportion among the calcium, silicon and aluminum oxides on currently used supplementary cementitious material compositions [17]. The equivalent region to red mud was obtained from a literature survey with the residue characteristics in different parts of the world, and the $CaO–SiO_2–Al_2O_3$ ratio from residue used in this work is featured. In case RM is confirmed as SCM, a new mineral addition class will be established.

As there is no technical standardization that can discuss the RM chemical properties, the obtained results lack a reference criterion. When materials containing silica and aluminum are in contact with water and calcium hydroxide, they generate stable compounds, known as pozzolans, but the red mud used in this work cannot be classified as a pozzolan, since the pozzolanic index, obtained by the Chapelle's method, was 385 mg of $Ca(OH)_2$ per gram of sample. Because the RM is a highly alkaline material, it affects the results due to the precipitation of calcium aluminate; another test was carried out with an RM solution of an approximately neutral pH, resulting in a pozzolanic index of 415 mg of $Ca(OH)_2$ per gram of sample. Results are lower than the Brazilian threshold to classify the material as a pozzolan.

Mineralogical compositions of cements are presented in Fig. 2, and the phases observed are indicated in Table 2.

The characteristic crystalline phases of clinker Portland (alite, belite, tri-calcium aluminate and brownmillerite), gypsum, calcite, quartz and periclase were found in all cements. Portlandite was also detected, showing a significant hydration of free lime.

A peak referring to hematite was observed in CPI, and the presence of dolomite was detected with siderophyllite as impurity in CPIIF. An amorphous halo referring to slag,

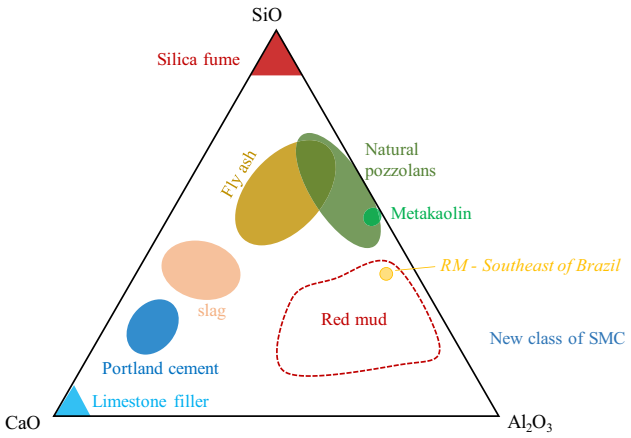

Fig. 1 Ternary diagram of $CaO–SiO_2–Al_2O_3$, indicating the ratio between the oxides on the currently used supplementary cementitious materials (SCM) compositions. In the case of RM, if that application is confirmed, it will be a new class of SCM

melilite and merwinite was observed in CPIII. Although not common in this type of cement, vesuvianite was also observed.

Figure 3 presents the diffractogram of red mud indicating the phases observed. Sodalite, produced by the digestion of bauxite ore with caustic soda, and the rock accessory minerals, as hematite, quartz, goethite, calcite, anatase, dicalcium silicate, a zeolitic phase of sodium aluminum silicate, and gibbsite, from incomplete digestion of the ore, were also observed.

Because cements chosen for this work present different chemical/mineralogical properties, it is expected that the interaction with red mud will be distinct.

Monitoring the chemical reaction and setting time of Portland cement

The chemical reaction of the Portland cement and the consequent released heat flow are directly dependent on material composition, use of supplementary materials, chemical admixtures, water content and other factors [19]. So, from the first contact with water, several simultaneous and consecutive reactions are started, an account for the chemical contribution to the hardened process over time.

The heat flow released during the chemical reaction of both pure cement and cement blended with red mud is shown in Fig. 4. The symbol (○) represents the setting time as determined by the Vicat test. The heat released was normalized according to cement content.

The use of mineral additions in association with Portland cement has two different effects on the kinetic of the hydration reaction, i.e., dilution of clinker phases and nucleation, which accentuate the precipitation of C–S–H and CH [17]. Then, this results in different heat released,

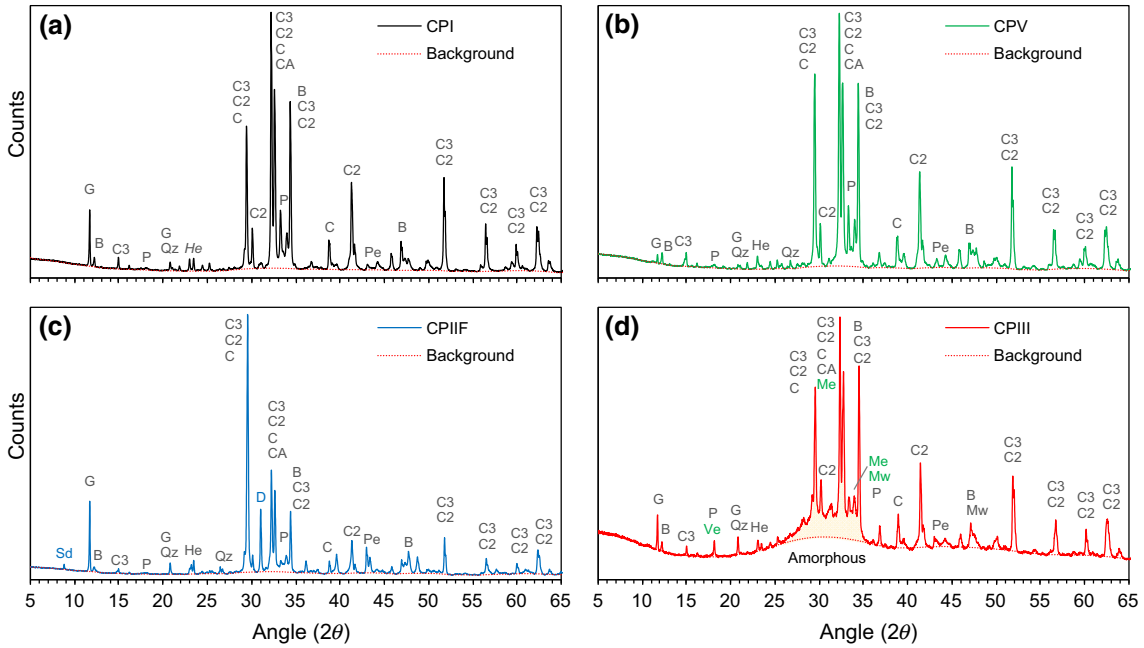

Fig. 2 Mineralogical composition of Brazilian Portland cements

Table 2 Mineralogical phases found in Portland cements used in this work

Represented by	Mineralogy	Molecular formulae	Consulted sheet	Find in
C3	Alite	$3CaO{\cdot}SiO_2$	ICOD 00-042-0551	All the cements
C2	Belite	$2CaO{\cdot}SiO_2$	ICOD 01-073-2091	All the cements
CA	Tri-calcium aluminate	$3CaO{\cdot}Al_2O_3$	ICOD 00-001-1060	All the cements
B	Brownmillerite	$4CaO{\cdot}Al_2O_3{\cdot}Fe_2O_3$	COD 96-900-3349	All the cements
C	Calcite	$CaCO_3$	ICOD 01-072-1651	All the cements
G	Gypsum	$CaSO_4{\cdot}2H_2O$	COD 96-101-0982	All the cements
Qz	Quartz	SiO_2	COD 96-900-9667	All the cements
Pe	Periclase	MgO	ICOD 01-077-2364	All the cements
P	Portlandite	$Ca(OH)_2$	ICOD 01-084-1273	All the cements
He	Hematite	Fe_2O_3	ICOD 00-013-0534	CPI
Sd	Siderophyllite	$K_2(Fe^{2+},Al)_6(Si,Al)_8O_{20}(OH)_4$	ICOD 01-079-1667	CPIIF
D	Dolomite	$(Ca,Mg)CO_3$	COD 96-900-1420	CPIIF
Me	Melilite	$(Al,Si)SiO_7$	COD 96-900-1290	CPIII
Mw	Merwinite	$Ca_3Mg(SiO_4)_2$	COD 96-900-0286	CPIII
Ve	Vesuvianite	$Ca_{10}(Mg,Fe)_2Al_4(SiO_4)_5(Si_2O_7)_2(OH,F)_4$	ICOD 01-079-2463	CPIII

according to each cement, and is more intense in the CPI and CPV, binders produced with higher amount of clinker.

A second inflexion after the peak of clinker phases reaction was observed in CPIII, indicating the slag reaction: The dissolution of clinker phases is a limiting parameter to the reaction rate and is affected by the ion concentration in solution [20]. In fact, it has been reported that Portland cement blended with a high amount of blast furnace slag undergoes a slow chemical reaction as compared to other types of cement, because the chemical reaction of slag occurs after the clinker.

To ease the understanding of results, the graphs presented in Fig. 4 were divided into 5 steps: peak of wetting, induction period, reaction rate, acceleration period and cumulative heat after 48 h of hydration. Table 3 shows the chemical reaction parameters as a function of each hydration stage; results illustrate that the use of red mud interferes in the same way on the periods evaluated.

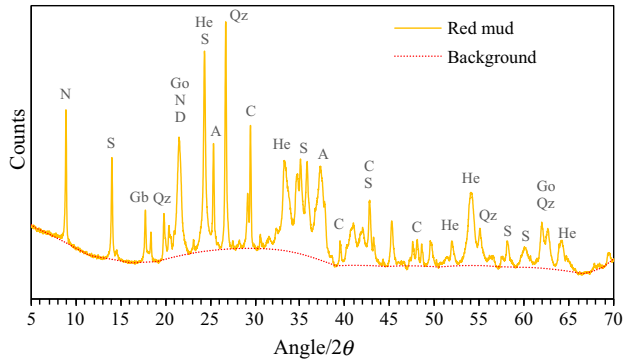

Fig. 3 Mineralogical composition of red mud used in this work. N—sodium aluminum silicate ($Na(AlSiO_4)$), S—sodalite ($(Na_4Al_3(SiO_4)_3Cl)$), Gb—gibbsite (γ-$Al(OH)_3$), Qz—quartz (SiO_2), Go—goethite ($FeO(OH)$), D—dicalcium silicate (Ca_2SiO_4), He—hematite (Fe_2O_3), A—anatase (TiO_2), C—calcite ($CaCO_3$)

In the wetting period, no specific tendency was observed in relation to the kind of Portland cement, but it is worth mentioning that there is an initial inertia in the stabilization of the ampoule temperature, causing some inaccuracy in the tests and doubtful results. However, there is a quick increase in the released heat due to the dissolution of the alkaline and calcium sulfates from anhydrous cement, i.e., K^+, Na^+, SO_4^{2-}, Ca^{2+} ions, saturating the solution.

The cement hydration reaction is directly related to the Ca^{2+} released, and the presence of red mud (and consequently, high amount of aluminates) changes the phase dissolution and the removal of part of calcium from the solution making all these systems increasingly complex.

Begarin et al. [21], evaluating the impact of Al (0,1%) on the chemical reaction of pure C_3S, observed a consid-

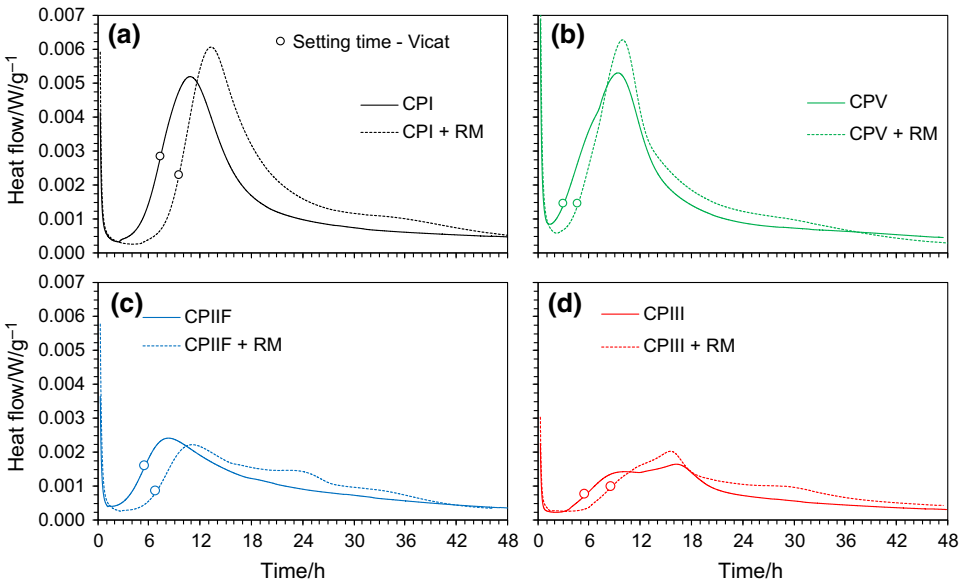

Fig. 4 Heat flow released during the chemical reaction of each cement, pure or blended with red mud. Symbol (○) represents the setting time as determined by the Vicat test

Table 3 Parameters of chemical reaction relating to each hydration stage

Sample	Wetting peak/ W g^{-1}	Induction period/ h:min	Reaction rate/ 10^{-4} W g^{-1} h^{-1}	Acceleration period/h:min	Peak of C–S–H and CH formation/ mW g^{-1}	Cumulative heat (48 h)/ J g^{-1}	Setting time (Vicat)/ h:min	Cumulative heat during the setting time/J g^{-1}
CPI	0.18	4:45	1.1	6:05	0.0052	263	7:40	25.0
CPI + RM	0.20	7:50	1.4	5:20	0.0061	316	9:30	22.9
CPV	0.17	2:25	0.7	7:00	0.0053	284	3:00	13.1
CPV + RM	0.14	3:50	0.9	6:05	0.0063	305	4:35	18.4
CPIIF	0.14	3:10	0.5	5:00	0.0024	186	5:25	15.4
CPIIF + RM	0.13	5:15	0.5	5:45	0.0022	198	6:50	13.8
CPIII	0.15	3:25	0.2	6:45	0.0014	144	5:25	7.4
CPIII + RM	0.18	5:50	0.2	9:40	0.0020	170	8:45	13.9

erable delay in the induction period, but there is no consensus about the effect of this ion on the kinetic of hydration. That concentration can affect the formation of hydrated products, also in accordance with results presented by *Quennoz and Scrivener* [22]. There is a hypothesis that the Al ion is incorporated into the C–S–H layer; another assumption is that the presence of Al ions poisons the C-S–H crystals in formation, etc. *Nicoleau, Schreiner and Nonat*, on the other hand, explained that the aluminate ions cause a strong inhibition of the dissolution due to the precipitation of an aluminosilicate species at the outermost surface of C_3S. Despite that, these Si–O–Al bonds are preferentially formed in low alkaline conditions; they are stabilized at higher pH by calcium ions in the coordination sphere of aluminum ions [23].

So, bauxite residue presents a high amount of sodium and aluminum in the form of sodium aluminate [$NaAl(OH)_4$], which, when in contact with Ca^{2+} ions dissociated from Portland cement, produces calcium aluminates and accelerates the heat flow in the beginning of the hydration reaction [17, 24–33].

However, the nucleation of C–S–H is slower in the presence of aluminates, as also reported by Garrault et al. [34], because the product precipitated at the beginning of hydration reaction, which contain Al ions, does not actuate as nucleation seeds. In parallel, with the dissolution of alkaline sulfates from the clinker of cements and calcium sulfates (setting regulators), the Al ions are quickly consumed by the AFt formation.

In fact, when this RM was used in association with Portland cement, an increase in the induction period was observed, accentuating, as it will be shown below, the formation of phases with aluminates, silicates and silicoaluminates. Aluminate ions, even at lower concentrations, exhibit an inhibitory effect which can affect the dissolution during the very early age of the hydration of C_3S. Definitely, during this short period of time, the conditions for making Si–O–Al bonds are met due to the rapid dissolution of aluminate anhydrous phases present in cement clinker, and this point is a factor influencing the time on the induction period [23]. The delay observed in this period varies in relation with the kind of binder, but it was more accentuated in the suspension with red mud and the purest binder (CPI).

Scrivener et al. [20] argued that the widely held theory of the formation of a protective layer on the surface of cement grains inhibiting further hydration was not in agreement with some experimental evidence and explained this period using a theory that they called as *geochemical theory of dissolution*. The essential aspect of this theory is that the dissolution is rapid at high degrees of undersaturation, as it is energetically favorable for etch pits to form. So, according to this theory, at a critical degree of undersaturation, the rate of dissolution slows dramatically, as etch pits can no longer form, or do not contribute as significantly, and dissolution is mainly restricted to step retreat.

The authors also pointed out that the surface becomes hydrated even before addition of the mixing water, due to inevitable exposure of the cement grains to humidity in the environment, changing the crystal structure, and this can explain why the surface energies calculated from the geochemical theory are less than those estimated from the anhydrous crystal structure. This altered layer remains throughout the hydration process, supporting the idea that these hydrated monomers correspond to the surface hydration, and the primary mechanism controlling the kinetics up to the end of the induction period is the undersaturation with respect to this surface layer.

Finally, but even without strong confirmation, as soon as the precipitation of C–S–H occurs, the concentration of Ca^{2+} ion in solution increases at the end of the induction period, in parallel with the dramatical drop in the concentration of silicate. Consequently, the rate of dissolution of C_3S becomes very slow as the solution is supersaturated with respect to calcium hydroxide. So, as the amount of product is small, it needs time to build as growth sites on the surface: It was suggested, then, that disorganized C–S–H starts to grow on the original grains and then needles start to grow out from these regions at the end of the induction period, starting the acceleration period and accentuating the heat released.

Independent of the theory applied to explain the induction period, it should be stressed that the results obtained in this work are not in accordance with a work carried out using another kind of red mud [17], in which that residue, with different physico-chemical properties, accentuated the nucleation effects on the cement chemical reaction and no delay was observed in the induction period. So, it is important to stress that the use of residues in association with cement may change from site to site, and a result obtained for a material from one place may not be similar to the results obtained to another kind of material.

In the sequence, the monitoring of heat flow in the acceleration period indicates that when RM is used in the composition, the purer the binder the higher is the reaction rate. Notwithstanding the impact of using RM in association with Portland cement, all the setting times occurred in the acceleration period are in conformity with the theory that the setting time may be related, in part, to the acceleration of C–S–H and CH formation, as defined in the ASTM C1679—13, *Standard Practice for Measuring Hydration Kinetics of Hydraulic Cementitious Mixtures Using Isothermal Calorimetry*.

The rate-determining mechanism in the acceleration period has long been attributed to the growth of C–S–H,

and there is considerable evidence to support this hypothesis. According to the geochemical dissolution theory, after the end of the induction period the system moves to a more dynamic equilibrium, and as soon as ions are removed from the solution by the precipitation of hydrates, the local undersaturation with respect to C_3S will go up, increasing the dissolution rate until the ions have been replaced in solution. For this reason, it was possible to have quite different dissolution rates for similar solution concentrations like presented in the pastes with different Portland cement with or without red mud.

In the deceleration period, the growing regions of hydrated product start to impinge and the surface available for growth decreases, so the formation of C–S–H and CH is still occurring, but it is slower. The deceleration of the reactions is also associated with the defects produced during precipitation that favor branching and gelation. At that stage, the formation of ettringite (AFt) and conversion in monosulfoaluminate (AFm), mainly in the Portland cements blended with red mud, were also observed, due to the presence of a large amount of aluminates.

The higher cumulative heat released after 48 h of hydration in the compositions with RM indicates that even with a delay in the induction period, the overall chemical reaction of Portland cement was intensified using this material.

Monitoring the formation of hydrated products over time

The main hydrated products formed are described below, using thermogravimetric analysis, X-ray diffraction and FTIR. An example of a differential thermogravimetric analysis—DTG result—is presented in Fig. 5 to illustrate how the main products obtained over time were quantified.

The thermal decomposition quantified up to 350 °C was considered as the free and bound water from the hydrated compounds of silicates, sulfates, aluminates and magnesium. Thus, in the following analysis the mass loss of gypsum, C–S–H, singenite, etc., was not differentiated [16].

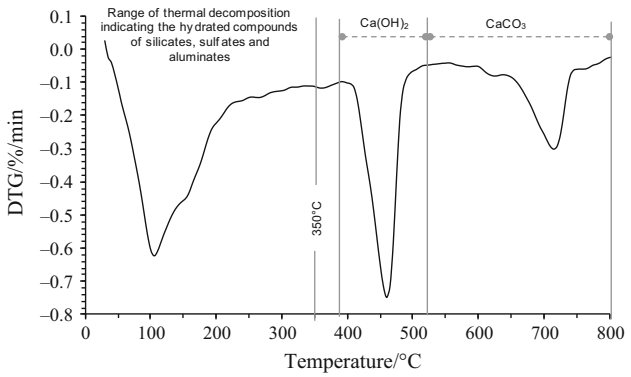

Fig. 5 Exemplification of the form used for the treatment of data from the DTG curve

The amount of portlandite ($Ca(OH)_2$) was mostly quantified between 360 and 480 °C, but that was not a fixed range for all evaluations and depended on the beginning and the end of the decomposition. The same form of evaluation was used for calcite quantification, in the characteristic temperature range for CO_2 release.

The percentages presented in the graphs for comparison of the weight loss at up to 350 °C are equivalent to the real data, that is, no multiplication factor was used, since the bound water loss occurred at the decomposition of different phases.

For portlandite, on the other hand, the percentage of decomposed water was multiplied by 4.11 ($MM_{Ca(OH)_2}/MM_{H_2O}$), and for calcite the percentage of decomposed CO_2 was multiplied by the 2.27 (MM_{CaCO_3}/MM_{CO_2}).

Figure 6 shows the formation process of the hydrated compounds from sulfates, silicates and aluminates: (a), (b), (c) and (d) present the result for the pastes with CPI, CPV, CPIIF and CPIII, respectively. Additionally, an illustration of the beginning of acceleration period during the hydration reaction, stage in which the evolution of chemical reaction is faster is presented. For all the pastes, the formation of hydrate compounds from the reactions with the sulfates, silicates and aluminates was lower in the pastes blended with red mud. For the CPI, CPV and CPIIF cements, this difference was maintained up to 48 h of monitoring, but for the CPIII, the impact of the use of RM could be clearly seen only up to 8 h of hydration reaction. As presented below in the discussion of the results of X-ray diffraction, with the use of the bauxite residue in association with Portland cement, the formation of C–S–H and NASH were intensified along with the formation of sodium aluminates. It is important to mention that in the first 4 h of hydration, the presence of gypsum is still observed, in the paste, but as explained previously, these products showed no differences in the thermogravimetric results.

Figure 7 shows the evolution of portlandite formation, and, as expected, an increase in the amount of this hydrated product over time was observed. However, the use of RM resulted in the quantification of a lower amount of portlandite than in the respective pure pastes, and the formation/consumption of this product is dependent on the kind of binder. Additionally, the formation of portlandite was intensified from the beginning of acceleration peak in every paste evaluated, with lower rate in the compositions with CPIII.

Considering that the peak of heat release presented in the isothermal conduction calorimetric analysis, related to

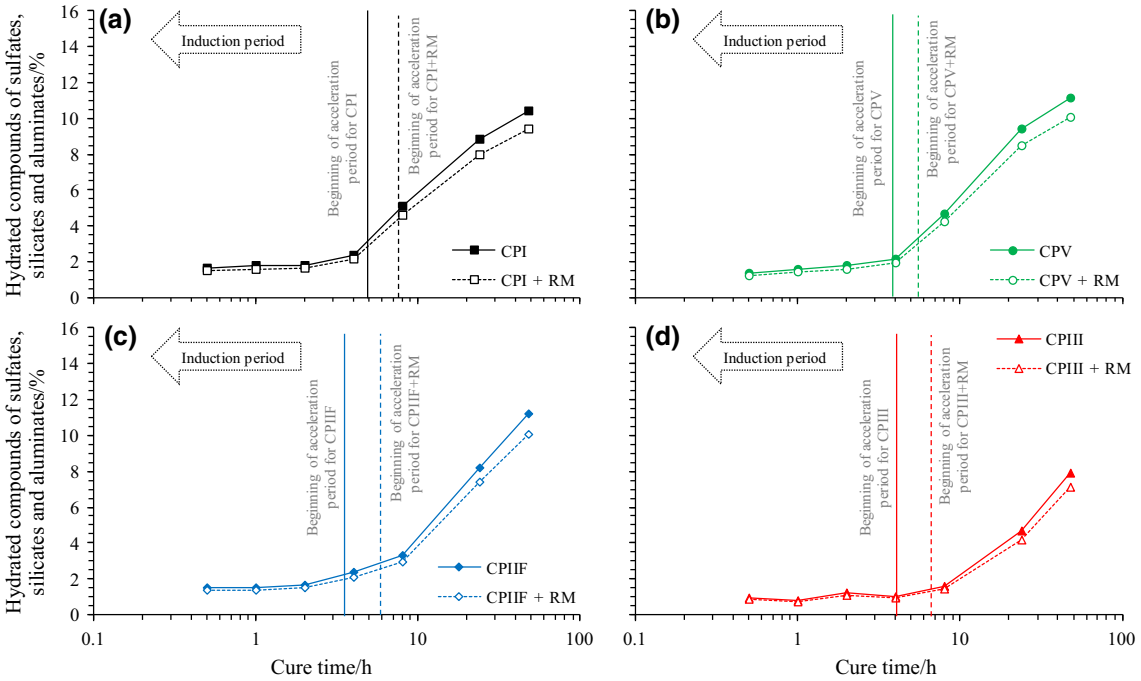

Fig. 6 Monitoring the formation of hydrates products from the sulfates, silicates, aluminates and magnesium compounds in the pastes with CPI (**a**), CPV (**b**), CPIIF (**c**) and CPIII (**d**). Values were normalized in function of amount of anhydrous cement

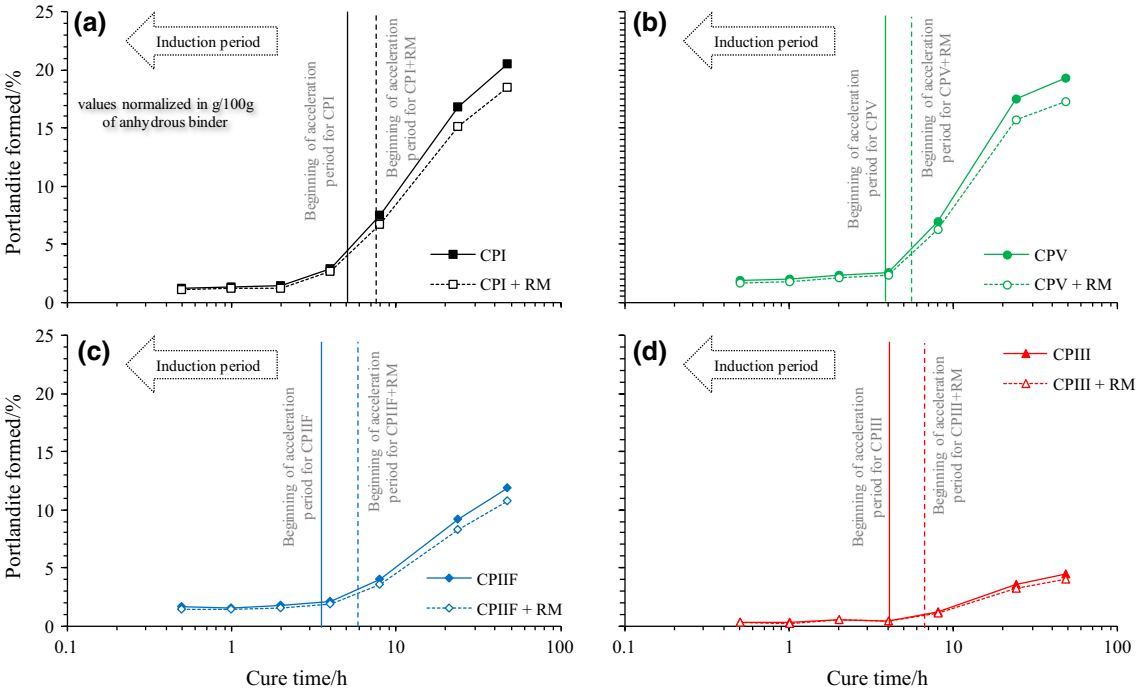

Fig. 7 Monitoring the formation of portlandite in the pastes with CPI (**a**), CPV (**b**), CPIIF (**c**) and CPIII (**d**). The values obtained in the test were multiplied by a 4.11 factor. Values were normalized in function of amount of anhydrous cement

the formation of C–S–H and CH, was more intense in the compositions with RM and given that in these formulations portlandite is consumed, the presence of RM resulted in a greater amount of hydrated calcium silicate, as shown previously, and it was confirmed by an X-ray diffraction analysis, presented as follows.

For the detection of calcite, on the other hand, the residue did not have any influence. As expected, the

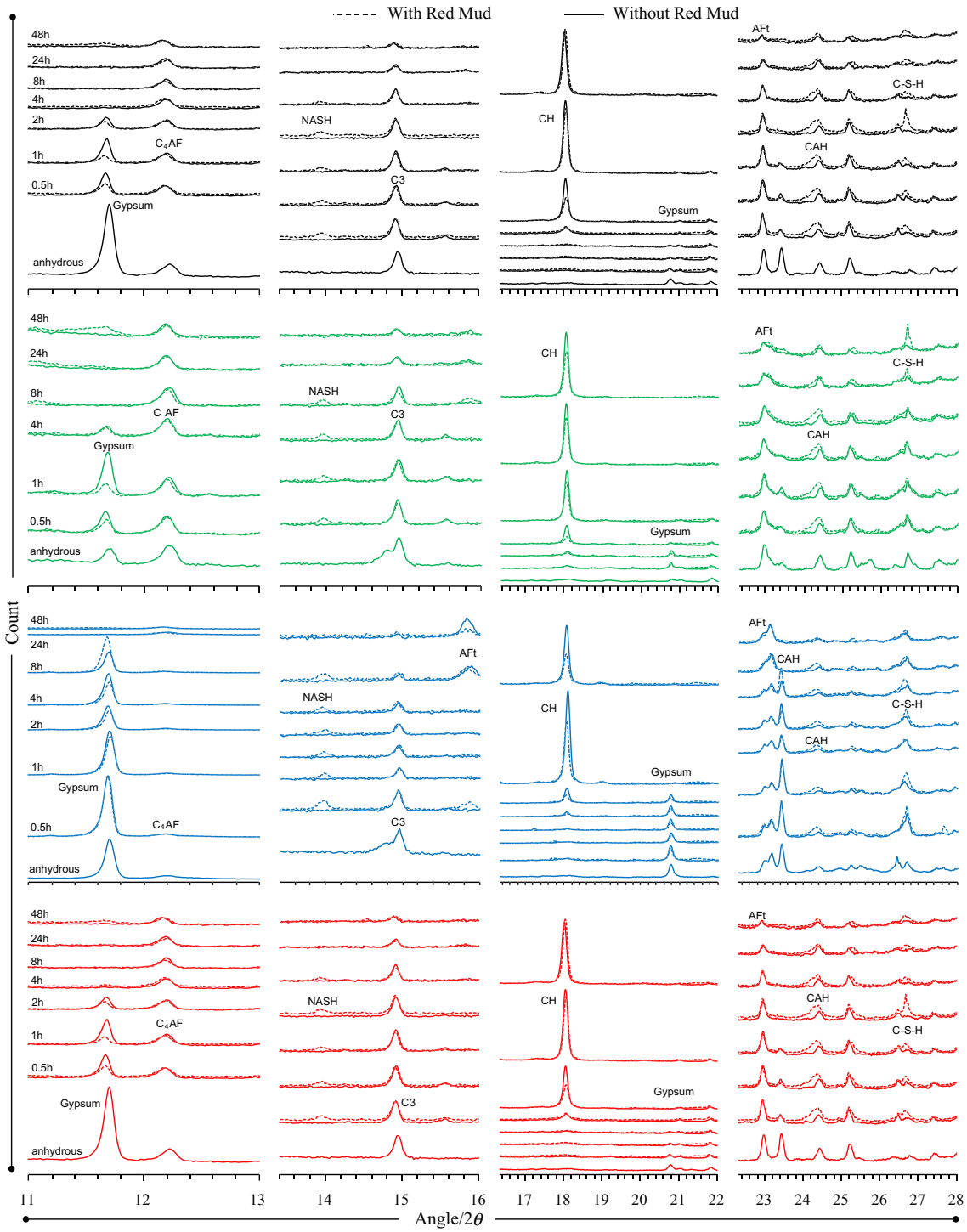

Fig. 8 Monitoring the hydrated phases formed in relation to the use of red mud. C–S–H—calcium silicate hydrate (ICDD 33-0306), CAH—calcium aluminate hydrate (COD 96-900-2390), AFt—ettringite (ICDD 41-1451), sodium/aluminate/silicate zeolite (COD 96-900-3328), CH—portlandite (COD 96-100-1788), Gypsum (COD 96-101-0982), C4AF (COD 96-900-3351), C3 (COD 96-900-8367)

highest amount of $CaCO_3$ was observed in the CPIIF, but the absolute increase in the calcite content, comparing the hydrated material for 30 min and after 48 h of hydration, was only about 2%. There is no evidence, from the characterization by thermal analysis, of the formation of carboaluminate phases up to 48 h of reaction. That fact was further confirmed by XRD, but it was detected only after 28 days of hydration or only for CPIIF after 7 days.

Contrary to what was expected at the outset of the work, no significant influence of the residue on the formation of

ettringite and calcium monosulfoaluminate (AFm) was observed from the XRD tests, although, from the calorimetric results presented previously, there is an acceleration in the Afm formation. In the evaluations performed for diffraction angles greater than 30° (2θ), no changes were observed in relation with the presence of residue in any of the cements studied.

Figure 8 illustrates the hydrated phases formed during the first 48 h of chemical reaction. The continuous lines indicate the suspensions which did not use red mud, and the dashed lines indicate the compositions containing red mud. From top to bottom, the corresponding results for CPI, CPV, CPIIF and CPIII are shown. Table 4 indicates the most important peak positions and mineralogical phases, highlighting some considerable differences between the compositions with and without the bauxite residue. In the evaluations performed for diffraction angles greater than 30° (2θ), no changes were observed in relation to the presence of the red mud:

1. The gypsum consumption (θ = 11.7°) is faster in the compositions with red mud due to the presence of a large amount of incorporated aluminates;
2. The peak related to portlandite (θ = 18.1°) is less intense, indicating that that compound is being consumed during the reaction;
3. The peak related to the formation of C–S–H (θ = 26.6°) is more intense, indicating the conversion of portlandite into calcium silicate hydrate;
4. The formation of calcium aluminate hydrate (θ = 24.5°) was accelerated due to the reaction of the aluminates of the residue with the Ca^{2+} ion dissociated from the cement; and.
5. Only in the compositions with red mud, independent of the kind of cement, a zeolitic sodium/aluminum/silicon phase was observed (θ = 13.9°).

No peaks related to the formation of AFm were observed from the XRD tests, although its formation has been shown by the calorimetric results presented previously; acceleration was observed in that formation. The poor crystallinity of this product can account for such result and this absent on the Afm detection by X-ray diffraction can be also explained by the method used to the stoppage of chemical reaction, being the better way to quantify ettringite, the stoppage using the immersion in isopropanol [18].

No evidence of calcium monocarboaluminate formation was found up to 48 h of reaction in any of the compositions. In theory, calcium carbonate should react with calcium aluminate forming the calcium carboaluminate phases in an analogous manner to the compounds hydrated with sulfate, i.e., AFt and AFm. However, due to the low solubility of $CaCO_3$, the reaction that produced monocarboaluminate was only observed after 7 days in the composition with CPIIF and after 28 days in the compositions with the other Portland cements.

Also, no evidences of U-phase ($CaO–Al_2O_3–SO_3–Na_2O–H_2O$) formation were noticed even with large amount of sodium and aluminates. However, in other works using the same red mud, it was observed considerable changes in the expansion after 28 days of cure, but it was not deeply evaluated correlating with the formation of U-phase system. In this case, the volumetric changes were attributed to ettringite formation.

A complementary evaluation of the hydrated products formed was carried out by infrared spectroscopy, and its results (Fig. 9) were divided into three regions, according to their wave number range [35–38]:

a. from 4000 to 2700 cm^{-1} referring mainly to the symmetrical (v_1) and asymmetrical (v_3) stretches of the O–H vibration of the sulfates and/or hydroxides and of the bands related to $CaCO_3$ added to the cement;

Table 4 Main peak positions and mineralogical phases found

Range	Peak position (2θ)	Assigned to	Observation
11° < 2θ < 13°	11.7°	Gypsum	*Lower* count in RM compositions
	12.2°	C_4AF	No influence of RM
13° < 2θ < 16°	13.9°	Sodium silicoaluminate hydrate—NASH	*Only* in RM compositions
	14.9°	Alite—C3	No influence of RM
16° < 2θ < 22°	18.1°	Portlandite—CH	*Lower* count in RM compositions
	20.9°	Gypsum	*Lower* count in RM compositions
22° < 2θ < 28°	22.9°	Ettringite—AFt	No influence of RM
	24.5°	Calcium aluminate hydrate—CAH	*Higher* count in RM compositions
	25.2°	Aluminum sulfate—AS	*Higher* count in RM compositions
	26.6°	C–S–H	*Higher* count in RM compositions

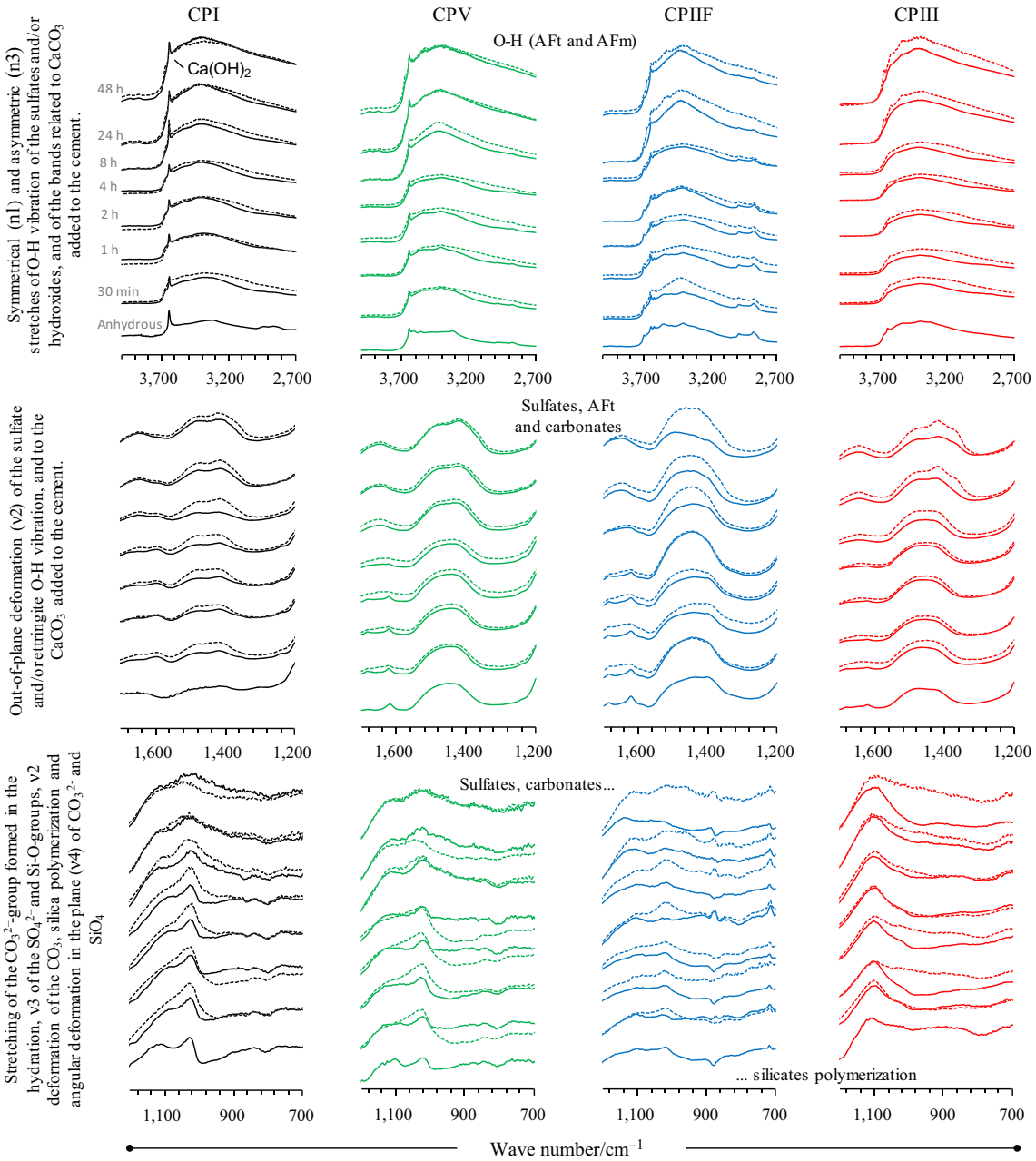

Fig. 9 Monitoring products formed by infrared spectroscopy

b. from 1700 to 1200 cm^{-1}, referring to the out-of-plane deformation (v_2) of the sulfates and/or ettringite O–H vibration and to the $CaCO_3$ added to the cement;
c. from 1200 to 700 cm^{-1}, indicating the stretching v_1 of the CO_3^{2-} group formed in the hydration, v_3 of the SO_4^{2-} and Si–O groups, v_2 deformation of the CO_3, silica polymerization and angular deformation in the plane (v_4) of CO_3^{2-} and SiO_4.

More specifically, that last brand brings new information about the hydration evolution of suspensions with and without red mud. So, differently from the other techniques used in that work, the FTIR indicated the formation of the hydrates, even if the hydrate was amorphous. Thus, these data complement the XRD results, that show only the crystalline minerals present, as well as the TG results, that cannot differentiate them.

The trends observed were the same for all suspensions, whether red mud was used or not, showing an increase in the intensity of vibrational bands as a function of curing time, due to the formation of hydrated products and the polymerization of silicates and carbonates.

The raise in the intensity over time in the bands between 3300 and 3700 cm^{-1} was more intense in the compositions with RM, attributed to the formation of $Ca(OH)_2$, ettringite and monosulfoaluminate. (The latter was observed in the calorimetry evaluation but not found using X-ray diffraction.)

From 1300 to 1600 cm^{-1}, there is a clear increase in the intensity referred to the O–H in the molecules of sulfates and ettringite, highlighting the higher intensity in the compositions with red mud.

Changes in the silicate's polymerization, from 1010 to 1080 cm^{-1}, and between 1100 and 1200 cm^{-1} were clearly identified and referred to the asymmetrical stretch of SO_4^{2-}, mainly in the compositions with red mud after 8 h of hydration. The fastest reaction during the first hours occurs because of ettringite formation. The portlandite formed afterward was partially consumed due to the interaction with silicates, resulting in C–S–H and NASH, as indicated by X-ray diffraction.

In addition, it can be inferred that the use of red mud brought about changes due to the formation of a higher amount of ettringite and AFm and a polymerizing reaction of carbonates and silicates. Therefore, even using this type of method for qualitative evaluations, it was possible to identify some differences caused by the use of red mud during the evolution of the hydration reaction of Portland cements.

Conclusions

Monitoring the chemical reaction of Portland cement in association with red mud was carried out by means of complementary methods.

The residue caused a delay in the induction period, resulting in a longer setting time, despite the increase in the final cumulative heat quantified after 48 h of monitoring. The presence of sodium aluminate in red mud contributes to a high amount of sodium and aluminum, which, when in contact with Ca^{2+} dissociated from Portland cement, results in calcium aluminates, accelerating the heat flow in the beginning of the hydration reaction. In parallel, with the dissolution of alkaline and calcium sulfates from the clinker, the Al ions are quickly consumed by the AFt in formation, resulting in longer induction period, intensifying the formation of phases with aluminates, silicates and silicoaluminates.

A higher amount of C–S–H, AFt, AFm and calcium aluminate hydrated in the compositions with red mud was also observed. However, only the FTIR results could indicate the formation of amorphous aluminosilicates hydrates, differently from the XRD and TG results.

Portlandite was also quickly consumed in the compositions with red mud, and sodium silicoaluminate hydrate—NASH, was observed only in the compositions with red mud.

Acknowledgements The authors wish to thank the Alcoa Foundation, the Laboratory of Microstructure and Eco-efficiency in Materials—LME, and CNPq—The National Council for Scientific and Technological Development (research grant—155357/2016-6) and FAPESP—The Foundation of Support to the Research of the State of São Paulo (research grant—2012/19262-2), for their financial support to this research work.

References

1. Scrivener KL, John VM, Gartner EM (2016) Eco-efficient cements: potential economically viable solutions for a low-CO_2 cement-based materials industry. United Nations Environment Programme.
2. Romano RCO, Bernardo HM, Niza DA, Mesquita JAFS, Cincotto MA, Pileggi RG. Evaluation of the hardened state properties of zero-cement mortars produced using bauxite residue as an activator to ground blast furnace slag. Athens: An Serbruyns; 2018. p. 293–300.
3. John VM, Damineli BL, Quattrone M, Pileggi RG. Fillers in cementitious materials: experience, recent advances and future potential. Cem Concr Res. 2018. https://doi.org/10.1016/j.cemconres.2017.09.013.
4. Damineli BL, John VM. Developing low CO_2 concretes: Is clinker replacement sufficient? The need of cement use efficiency improvement. Key Eng Mater. 2012;517:342–51.
5. Romano RCO, Mesquita JAFS, Bernardo HM, Brasileiro GCP, Muniz GHU, Cincotto MA, Pileggi RG. Impact of using bauxite residue in microconcrete and comparison with other kind of supplementary cementitious material. Hamburg: Travaux ICSOBA; 2017. p. 505–18.
6. de Oliveira Romano RC, Liberato CC, Montini M, Gallo JB, Cincotto MA, Pileggi RG. Evaluation of transition from fluid to elastic solid of cementitious pastes with bauxite residue using oscillation rheometry and isothermal calorimetry. Appl Rheol. 2013;23:23830.
7. Roth J, Falter J. Potential commercial processes for the utilization of bauxite residues. In: 35th Conference on exhibit. ICSOBA—bauxite alumina and aluminium industry European New Global Development ICSOBA, Hamburg; 2017. p. 539–546.
8. Arnout L, Hertel T, Liard M, Lootens D, Pontikes Y. Use of bauxite residue slurry as single activator in a hybrid binder system. In: 35th Conference on exhibit. ICSOBA—bauxite alumina and aluminium industry European New Global Development ICSOBA, Hamburg; 2017. p 519–528.
9. Gräfe M, Power G, Klauber C. Bauxite residue issues: III. Alkalinity and associated chemistry. Hydrometallurgy. 2011;108:60–79.
10. Pontikes Y, Nikolopoulos P, Angelopoulos GN. Thermal behaviour of clay mixtures with bauxite residue for the production of heavy-clay ceramics. J Eur Ceram Soc. 2007;27:1645–9.
11. Wang S, Ang HM, Tadé MO. Novel applications of red mud as coagulant, adsorbent and catalyst for environmentally benign processes. Chemosphere. 2008;72:1621–35.
12. Cooling DJ, Hay PS, Guilfoyle L. Carbonation of bauxite residue. In: Proceedings of 6th international alumina quality workshop, Brisbane; 2002. p. 185–190.

13. Kasliwal P, Sai PST. Enrichment of titanium dioxide in red mud: a kinetic study. Hydrometallurgy. 1999;53:73–87.
14. Sujana MG, Thakur RS, Acharya BC, Das SN, Rao SB. Effect of calcination and physico-chemical properties of red mud; 1996.
15. Klauber C, Gräfe M, Power G. Bauxite residue issues: II. Options for residue utilization. Hydrometallurgy. 2011;108:11–32.
16. Romano RCO. Avaliação das interações físico-químicas entre resíduo de bauxita e cimento Portland; 2016.
17. Romano RCO, Bernardo HM, Maciel MH, Pileggi RG, Cincotto MA. Hydration of Portland cement with red mud as mineral addition. J Therm Anal Calorim. 2018;131:2477–90.
18. Maciel MH, Soares GS, de Oliveira Romano RC, Cincotto MA. Monitoring of Portland cement chemical reaction and quantification of the hydrated products by XRD and TG in function of the stoppage hydration technique. J Therm Anal Calorim. 2018. https://doi.org/10.1007/s10973-018-7734-5.
19. Fujii AL, dos Reis Torres D, de Oliveira Romano RC, Cincotto MA, Pileggi RG. Impact of superplasticizer on the hardening of slag Portland cement blended with red mud. Constr Build Mater 101 Part. 2015;1:432–9.
20. Scrivener KL, Juilland P, Monteiro PJM. Advances in understanding hydration of Portland cement. Cem Concr Res. 2015;78:38–56.
21. Begarin F, Garrault S, Nonat A, Nicoleau L. Hydration of alite containing aluminium. Adv Appl Ceram. 2011;110:127–30.
22. Quennoz A, Scrivener KL. Interactions between alite and C3A-gypsum hydrations in model cements. Cem Concr Res. 2013;44:46–54.
23. Nicoleau L, Schreiner E, Nonat A. Ion-specific effects influencing the dissolution of tricalcium silicate. Cem Concr Res. 2014;59:118–38.
24. Bentz DP. Modeling the influence of limestone filler on cement hydration using CEMHYD3D. Cem Concr Compos. 2006;28:124–9.
25. De Weerdt K, Haha MB, Le Saout G, Kjellsen KO, Justnes H, Lothenbach B. Hydration mechanisms of ternary Portland cements containing limestone powder and fly ash. Cem Concr Res. 2011;41:279–91.
26. Duchesne J, Be MA. Effect of supplementary cementing materials on the composition of cement hydration products. Adv Cem Based Mater. 1995;2:43–52.
27. Snellings R, Mertens G, Cizer Ö, Elsen J. Early age hydration and pozzolanic reaction in natural zeolite blended cements: reaction kinetics and products by in situ synchrotron X-ray powder diffraction. Cem Concr Res. 2010;40:1704–13.
28. Elgalhud AA, Dhir RK, Ghataora G. Limestone addition effects on concrete porosity. Cem Concr Compos. 2016;72:222–34.
29. Ramezanianpour AM, Hooton RD. A study on hydration, compressive strength, and porosity of Portland-limestone cement mixes containing SCMs. Cem Concr Compos. 2014;51:1–13.
30. Singh M, Upadhayay SN, Prasad PM. Preparation of special cements from red mud. Waste Manag. 1996;16:665–70.
31. Kumar R, Bhattacharjee B. Porosity, pore size distribution and in situ strength of concrete. Cem Concr Res. 2003;33:155–64.
32. Tsakiridis PE, Agatzini-Leonardou S, Oustadakis P. Red mud addition in the raw meal for the production of Portland cement clinker. J Hazard Mater. 2004;116:103–10.
33. Zhang J, Weissinger EA, Peethamparan S, Scherer GW. Early hydration and setting of oil well cement. Cem Concr Res. 2010;40:1023–33.
34. Garrault S, Nonat A, Sallier Y, Nicoleau L. On the origin of the dormant period of cement hydration. In: XVIII international congress on cement chemistry; 2011.
35. Hughes TL, Methven CM, Jones TGJ, Pelham SE, Fletcher P, Hall C. Determining cement composition by Fourier transform infrared spectroscopy. Adv Cem Based Mater. 1995;2:91–104.
36. Mollah MYA, Kesmez M, Cocke DL. An X-ray diffraction (XRD) and Fourier transform infrared spectroscopic (FT-IR) investigation of the long-term effect on the solidification/stabilization (S/S) of arsenic(V) in Portland cement type-V. Sci Total Environ. 2004;325:255–62.
37. Trezza MA, Lavat AE. Analysis of the system $3CaO{\cdot}Al_2O_3$–$CaSO_4{\cdot}2H_2O$–$CaCO_3$–H_2O by FT-IR spectroscopy. Cem Concr Res. 2001;31:869–72.
38. Ylmén R, Jäglid U, Steenari B-M, Panas I. Early hydration and setting of Portland cement monitored by IR, SEM and Vicat techniques. Cem Concr Res. 2009;39:433–9.

Publisher's Note Springer Nature remains neutral with regard to jurisdictional claims in published maps and institutional affiliations.